

# TINYIO: LIGHTWEIGHT REPARAMETERIZED INERTIAL ODOMETRY

Shanshan Zhang<sup>\*†</sup>Siyue Wang<sup>\*</sup>Liqin Wu<sup>\*</sup>Qi Zhang<sup>\*</sup>Tianshui Wen<sup>\*</sup> Ziheng Zhou<sup>\*</sup>

Ao Peng

<sup>\*</sup> Department of Information and Communication Engineering, Xiamen University<sup>†</sup> Department of Electronic Science, Xiamen University, China<sup>‡</sup> Corresponding author, lxzheng@xmu.edu.cn, yuyang15@xmu.edu.cn

## ABSTRACT

Inertial odometry (IO) is a widely used approach for localization on mobile devices; however, obtaining a lightweight IO model that also achieves high accuracy remains challenging. To address this issue, we propose TinyIO, a lightweight IO method. During training, we adopt a multi-branch architecture to extract diverse motion features more effectively. At inference time, the trained multi-branch model is converted into an equivalent single-path architecture to reduce computational complexity. We further introduce a sparse gating unit that suppresses noise via element-wise selection and integrates contextual motion cues with local, fine-grained features. Extensive experiments on public benchmarks demonstrate that our method attains a favorable trade-off between accuracy and model size. On the RoNIN dataset, TinyIO reduces the ATE by 2.59% compared with RoNIN ResNet and decreases the parameter count by 3.86%.

**Index Terms**— Reparameterization, Lightweight, Inertial Measurement Unit signals, Inertial Odometry

## 1. INTRODUCTION

Inertial odometry (IO) aims to estimate a platform’s position over time from inertial measurement unit (IMU) signals [1]. An IMU typically comprises accelerometers and gyroscopes, which measure linear acceleration and angular velocity, respectively. Owing to their low power consumption and inherent protection of data privacy, IO has been widely adopted in assistive localization for individuals with disabilities, positioning of IoT devices [2, 3], and ambient-assisted living [4–6].

IO methods can generally be categorized into two types: Newtonian-mechanics-based approaches and data-driven approaches. Traditional methods grounded in Newtonian mechanics offer the advantage of low computational overhead; however, they suffer from cumulative errors, and are often constrained by environment-specific factors, which limit their practical applicability [7–9].

In contrast, data-driven IO methods learn motion patterns directly from IMU signals to estimate position. These methods typically achieve higher localization accuracy and exhibit

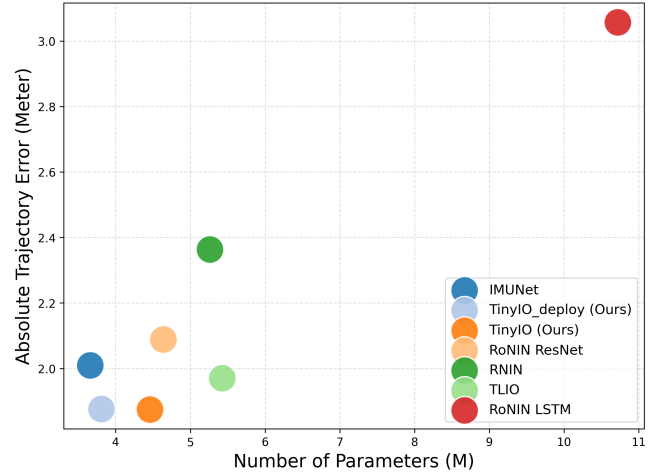


**Fig. 1:** Comparison of ATE performance across different models on the RNIN dataset. Each point corresponds to an IO algorithm; points closer to the bottom-left corner indicate lower trajectory error with fewer model parameters. The proposed methods, Tiny and Tiny\_deploy, achieve the lowest ATE while maintaining a compact parameter size.

improved generalization across diverse environments [5, 10–13]. Nevertheless, many existing approaches emphasize accuracy by employing large-scale models while overlooking the importance of lightweight models for IO, particularly for mobile deployment [2, 3].

To address this issue, we propose a lightweight IO framework named TinyIO, which decouples the training and inference phases to enhance parameter efficiency. The main contributions of this paper are as follows:

- We perform inference-time reparameterization to decouple the model from its training architecture, thereby improving parameter efficiency.
- We introduce a sparse gating unit that suppresses noise in IMU signals while effectively fusing contextual motion information with local fine-grained features.
- Experimental results on multiple public datasets demonstrate that TinyIO achieves a favorable trade-off between accuracy and parameters, as illustrated in Fig. 1.

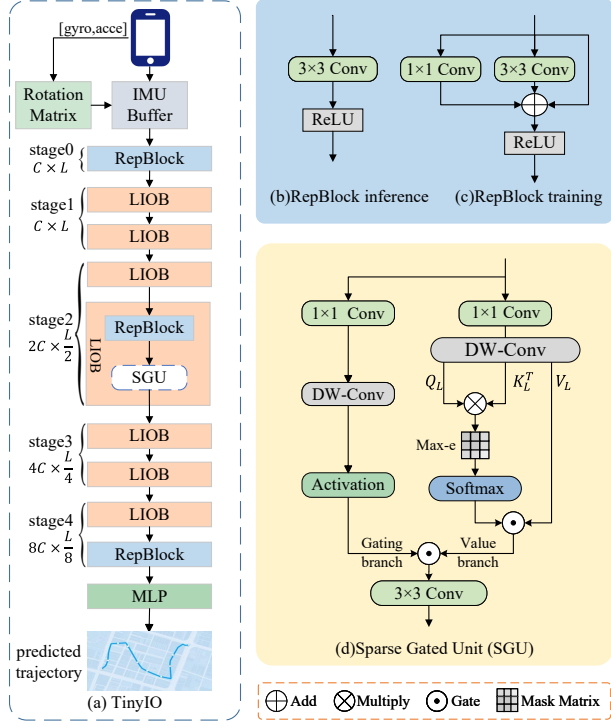


Fig. 2: Schematic diagram of the proposed TinyIO architecture.

## 2. METHOD

### 2.1. Overall Pipeline

The overall pipeline of the proposed TinyIO, illustrated in Fig. 2(a), employs a symmetric architecture. The TinyIO backbone comprises seven stacked Lightweight Inertial Odometry Blocks (LIOBs), with two Reparameterization Blocks (RepBlocks) placed at the input and output for channel alignment. These modules are arranged into five stages to extract rich motion information.

Each LIOB contains a RepBlock and a Sparse Gated Unit (SGU). The RepBlock adopts a multi-branch structure to capture complex motion patterns during training. At inference time, this multi-branch structure is reparameterized into an equivalent single-path feedforward form to improve parameter efficiency, as shown in Fig. 2(b). Feature fusion is performed by the SGU, which applies sparse attention [14, 15] to suppress noise by selectively filtering elements, and fuses contextual motion information with local fine-grained features via a gating mechanism (see Fig. 2(d)).

Finally, a multi-layer perceptron (MLP) head predicts velocity; the network is trained by minimizing the mean squared error (MSE) loss.

### 2.2. Lightweight Inertial Odometry Block

To balance model complexity and accuracy, we incorporate reparameterization techniques into the Lightweight Inertial Odometry Blocks (LIOBs) and introduce a sparse gating mechanism. Given an IMU signal  $\mathbf{X} \in \mathbb{R}^{C \times F}$ , where  $C = 6$

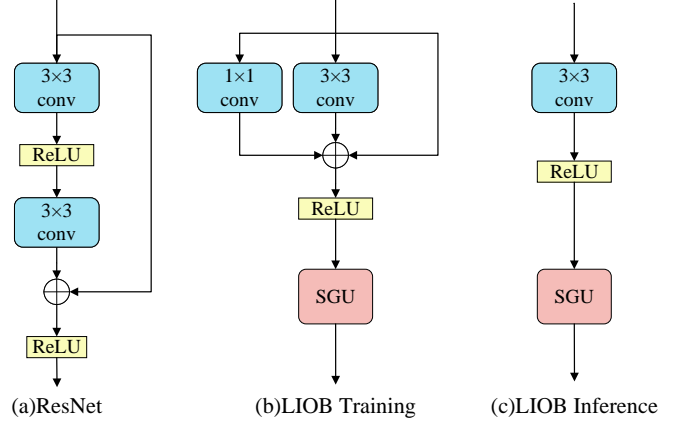


Fig. 3: Comparison of the basic modules of LIOB and ResNet.

denotes the six channels from the three-axis accelerometer and gyroscope and  $F$  denotes the number of frames per time window (i.e., the IMU sampling rate), the processing within each LIOB is:

$$\begin{aligned} \mathbf{X}' &= \text{RepBlock}(\mathbf{X}), \\ \mathbf{X}'' &= \text{SGU}(\mathbf{X}'). \end{aligned} \quad (1)$$

Here,  $\mathbf{X}'$  and  $\mathbf{X}''$  denote the outputs of the RepBlock and the SGU, respectively.

**Reparameterization Block (RepBlock).** The RepBlock is a core component of each LIOB and is also applied at both the beginning and the end of the backbone for channel alignment. To improve parameter efficiency and enhance feature extraction, the RepBlock decouples the training and inference architectures [16]. Fig. 3 illustrates the structural differences between the RepBlock and the core block used in the RoNIN ResNet backbone.

During training, a multi-branch architecture—similar to that of ResNet—is adopted to extract features from the IMU signal. Specifically, the computation within each RepBlock during training is given by

$$\mathbf{Y} = \mathbf{X} + \phi(\mathbf{X}) + \psi(\mathbf{X}) \in \mathbb{R}^{C \times F}, \quad (2)$$

where  $\mathbf{X}$  denotes the input to the block, and  $\phi(\cdot)$  and  $\psi(\cdot)$  denote 1D convolutional branches with kernel sizes 3 and 1, respectively.

At inference, the multi-branch structure is reparameterized into a single-path connection, as shown in Fig. 3(c). This transformation preserves the equivalence of the learned parameters while simplifying the architecture, thereby improving computational efficiency without degrading predictive accuracy. At inference time the operation is represented as

$$\mathbf{Y} = \gamma(\mathbf{X}) \in \mathbb{R}^{C \times F}, \quad (3)$$

where  $\gamma(\cdot)$  denotes a single 1D convolution (kernel size 3) obtained by merging the parameters of  $\phi(\cdot)$ ,  $\psi(\cdot)$ , and the residual (identity) connection from the training phase.

**Sparse Gated Unit (SGU).** While the RepBlock emphasizes local fine-grained motion features, it lacks sufficient

**Table 1:** Comparison of trajectory prediction performance, ablation studies, and model efficiency. For comparison (left of dashed line), the best results are highlighted in **bold**. For ablation studies (right of dashed line), the best results are underlined. Parameters and FLOPs: the best results are highlighted in **bold**. ATE and RTE are measured in meters. Parameters and FLOPs are reported in millions.

Dataset	Metric	RoNIN ResNet	RoNIN LSTM	RNIN	IMUNet	TLIO	TinyIO_deploy	TinyIO	TinyIO vs RoNIN ResNet	Ablation Study	
										TinyIO (w/o SGU)	Full TinyIO
RoNIN	ATE	4.043	6.070	7.352	4.093	11.778	4.081	<b>3.939</b>	2.59%	4.288	3.939
	RTE	3.123	3.588	3.420	2.859	3.856	<b>2.806</b>	2.857	8.50%	3.175	<u>2.857</u>
RIDI	ATE	1.987	5.208	2.259	2.180	2.347	1.980	<b>1.718</b>	13.54%	1.860	<u>1.718</u>
	RTE	2.125	5.540	2.426	2.366	2.291	2.123	<b>1.927</b>	9.33%	1.990	<u>1.927</u>
RNIN	ATE	2.089	3.057	2.364	2.010	1.970	1.876	<b>1.875</b>	10.25%	2.085	<u>1.875</u>
	RTE	1.819	3.264	2.536	1.876	1.785	1.732	<b>1.731</b>	4.82%	1.802	<u>1.731</u>
TLIO	ATE	1.601	2.144	1.653	1.609	2.442	1.617	<b>1.459</b>	8.85%	1.560	<u>1.459</u>
	RTE	3.968	5.263	4.132	4.113	6.799	4.135	<b>3.637</b>	8.33%	3.916	<u>3.637</u>
-	FLOPs (M)	38.252	54.023	72.032	<b>18.838</b>	39.436	49.379	60.968	-	-	-
-	Param (M)	4.635	10.719	5.259	<b>3.659</b>	5.424	3.809	4.459	-	-	-

contextual awareness. To address this limitation, we introduce the SGU, which suppresses noise through element-wise filtering and integrates contextual motion information with local details to enable multi-scale feature interaction. The SGU structure is illustrated in Fig. 2(d). It comprises two branches: a value branch that captures contextual dependencies via sparse attention, and a gating branch that captures local fine-grained variations.

In the value branch, we apply a standard 1D convolution and a depthwise 1D convolution (followed by a transpose) to produce keys  $K$ , queries  $Q$ , and values  $V$ , where  $K, Q, V \in \mathbb{R}^{F \times C}$ . We then compute the attention score matrix  $\frac{QK^T}{\sqrt{C}} \in \mathbb{R}^{F \times F}$ , which captures pairwise dependencies among frames. To reduce spurious dependencies and suppress noise [15], we apply a max- $e$  sparsification that retains only the top  $e$  fraction of elements in each row. (In our experiments we set  $e = 0.8$ , i.e., retain the top 80% of elements per row.) The sparse score matrix is normalized row-wise by a softmax and then applied to  $V$  to obtain the attention output:

$$\text{Value} = \text{Softmax}\left(\max-e\left(\frac{K^T Q}{\sqrt{C}}\right)\right) V \in \mathbb{R}^{F \times C}. \quad (4)$$

The gating branch applies a depthwise convolution followed by a nonlinear activation to capture local, channel-wise motion variations. This branch functions equivalently to a gated channel-attention module and increases sensitivity to subtle motion cues that the value branch may overlook.

Finally, the outputs of the value and gating branches are fused via the gating mechanism to facilitate multi-scale feature integration while suppressing implicit noise. The SGU is a versatile module suitable for a range of inertial localization scenarios.

### 3. EXPERIMENTS AND ANALYSIS

#### 3.1. Experimental Settings

**Training details.** All training and evaluation procedures are carried out on a single NVIDIA RTX 3090 GPU with 24 GB of memory. The network is optimized using the Adam optimizer with an initial learning rate of  $10^{-4}$ . Training runs

for up to 100 epochs, with early stopping triggered when the learning rate decays below  $10^{-6}$ . The channel dimensions of TinyIO’s five stages are set to [64, 64, 128, 256, 512].

**Datasets and metrics.** We evaluate on four widely used open-source datasets: RIDI [17], RoNIN [18], RNIN [19], and TLIO [20]. Each dataset is split into training, validation, and test subsets with a ratio of 8:1:1, and all models are retrained on the respective datasets for fair comparison. Three evaluation metrics are used: absolute trajectory error (ATE) [21], relative trajectory error (RTE) [21], and position drift error (PDE) [22]. ATE quantifies global trajectory consistency, RTE measures local trajectory drift, and PDE evaluates endpoint deviation.

**Baselines.** Prior work has shown that data-driven approaches typically outperform Newtonian model-based methods in localization accuracy [17, 19, 20, 23, 24]. Accordingly, we compare TinyIO against representative data-driven baselines: the ResNet and LSTM architectures from RoNIN [18], the network designs of RNIN [19] and TLIO [20], and the lightweight IMUNet architecture [2].

#### 3.2. Comparisons with the baselines

**Metric evaluation.** Table 1 (left) summarizes ATE and RTE comparisons between TinyIO and the baseline models. TinyIO and its reparameterized variant, TinyIO\_deploy, achieve the lowest localization errors in most scenarios. For example, relative to RoNIN ResNet, TinyIO reduces ATE by 2.59%—13.54% and RTE by 4.82%—9.33% across the four datasets. Model complexity increases progressively from RoNIN to TLIO and RNIN, which raises deployment challenges for edge devices. Although IMUNet uses depthwise-separable convolutions to reduce complexity, its localization accuracy remains limited. In contrast, TinyIO decouples training and inference to substantially reduce parameter counts, while the SGU suppresses implicit noise and fuses local fine-grained and contextual motion features to strike an effective balance between accuracy and compactness. Overall, these improvements explain the superior performance of TinyIO over the baselines.

**Visualization.** Fig. 5 shows a comparison of PDE among TinyIO, TinyIO\_deploy, and RoNIN (results on the RoNIN

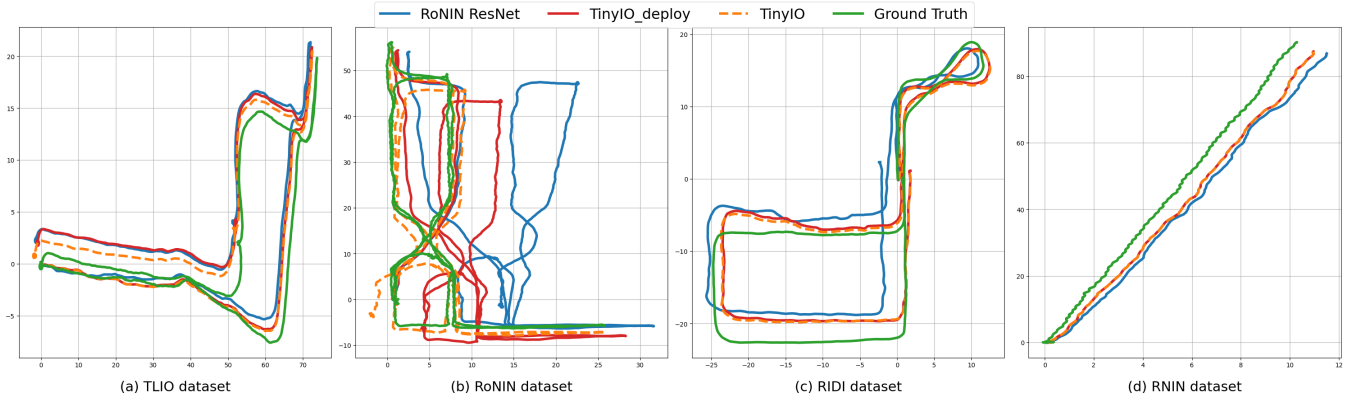


Fig. 4: Visual comparison of TinyIO and RoNIN ResNet on various datasets.

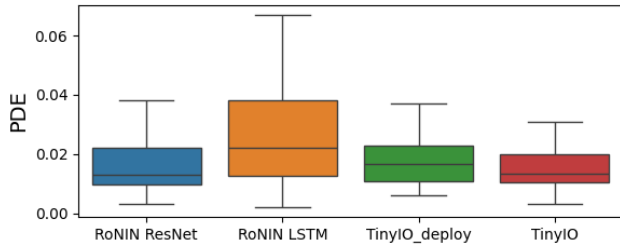


Fig. 5: PDE comparison between TinyIO and three baseline models from RoNIN on the RoNIN dataset.

dataset are shown due to space constraints). TinyIO attains the smallest PDE median and the most compact error distribution, indicating superior endpoint approximation. Although reparameterization slightly increases PDE for TinyIO\_deploy, TinyIO\_deploy still outperforms RoNIN ResNet and preserves high-fidelity trajectory reconstruction consistent with the training-phase model.

Fig. 4 visualizes trajectory reconstructions produced by TinyIO and the baseline models on the test sets. In Fig. 4(d), TinyIO effectively captures contextual motion information, yielding accurate and stable tracking. After reparameterization, the positioning error of TinyIO\_deploy increases slightly but remains lower than that of RoNIN ResNet, suggesting that the accuracy degradation due to reparameterization is within acceptable bounds. For complex trajectories (Fig. 4(a)–(c)), TinyIO better models local fine-grained motion and exhibits substantially less drift than RoNIN ResNet when handling rotational or highly nonlinear motions; consequently, both TinyIO and TinyIO\_deploy closely follow ground-truth trajectories, whereas RoNIN ResNet shows pronounced drift during turns and increasingly larger deviations as trajectory complexity grows.

### 3.3. Ablation study

We conduct ablation experiments to validate the reparameterization strategy and the contributions of individual modules (SGU and RepBlock).

The middle section of Table 1 reports performance comparisons between TinyIO and TinyIO\_deploy across the

four datasets. After reparameterization, TinyIO\_deploy (3.809M parameters) reduces the parameter count by approximately 14.52% relative to TinyIO (4.456M), and its model size is only 82.18% that of RoNIN ResNet (4.635M). Despite this compression, the increases in ATE and RTE for TinyIO\_deploy are marginal, and TinyIO\_deploy still outperforms RoNIN ResNet in localization accuracy. Visualization results in Fig. 4 corroborate these findings. These results indicate that the proposed reparameterization achieves a favorable trade-off between parameters and accuracy, making TinyIO particularly suitable for edge devices with limited storage.

The right portion of Table 1 shows module ablation results. Removing SGU (TinyIO w/o SGU) leaves only the RepBlock: the model still captures local fine-grained motion and yields substantially lower localization error than RoNIN ResNet, indicating that RepBlock both reduces parameter complexity and contributes positively to accuracy. Integrating SGU into the full TinyIO architecture further improves accuracy, demonstrating that multi-scale feature fusion via SGU is critical for enhanced trajectory estimation. These findings confirm the effectiveness and complementarity of the proposed components.

## 4. CONCLUSION

We present TinyIO, a lightweight IO framework that attains a favorable trade-off between localization accuracy and model parameters. In practical deployment, however, additional procedures such as model fine-tuning may be necessary to adapt to previously unseen carrier motion patterns.

## 5. ACKNOWLEDGEMENTS

This work is supported by Science and Technology Major Program of Fujian Province (No. 2022HZ026007) and partly supported by the Science and Technology Planning Project of Fujian province (2022I0001).

## 6. REFERENCES

- [1] R. Harle, “A survey of indoor inertial positioning systems for pedestrians,” *IEEE Commun. Surv. Tutorials*, vol. 15, no. 3, pp. 1281–1293, 2013.
- [2] B. Zeinali, H. Zanddizari, and M. J. Chang, “Imunet: Efficient regression architecture for inertial imu navigation and positioning,” *IEEE Trans. Instrum. Meas.*, vol. 73, no. 2516213, 2024.
- [3] O. Tariq, B. Dastagir, M. Bilal, and D. Han, “Deepils: Towards accurate domain invariant aiot-enabled inertial localization system,” *IEEE Internet Things J.*, pp. 1–1, 2025.
- [4] A. K. Panja, C. Chowdhury, and S. Neogy, “Survey on inertial sensor-based ils for smartphone users,” *CCF Trans. Pervasive Comput. Interact.*, vol. 4, no. 3, pp. 319–337, 2022.
- [5] X. Cao, C. Zhou, D. Zeng, and Y. Wang, “Rio: Rotation-equivariance supervised learning of robust inertial odometry,” in *CVPR*, 2022, pp. 6604–6613.
- [6] S. Herath, D. Caruso, C. Liu, Y. Chen, and Y. Furukawa, “Neural inertial localization,” in *CVPR*, 2022, pp. 6594–6603.
- [7] P. G. Savage, “Strapdown inertial navigation integration algorithm design part 2: Velocity and position algorithms,” *J. Guid. Control Dyn.*, vol. 21, no. 2, pp. 208–221, 1998.
- [8] M. Kourogi and T. Kurata, “A method of pedestrian dead reckoning for smartphones using frequency domain analysis on patterns of acceleration and angular velocity,” in 2014 IEEE/ION Posit. Locat. Navig. Symp.-PLANS 2014. IEEE, 2014, pp. 164–168.
- [9] H. Li, H. Liu, Z. Li, C. Li, Z. Meng, N. Gao, and Z. Zhang, “Adaptive threshold-based zupt for single imu-enabled wearable pedestrian localization,” *IEEE Internet Things J.*, vol. 10, no. 13, pp. 11749–11760, 2023.
- [10] S. Zhao, S. Zhou, R. Blanchard, Y. Qiu, W. Wang, and S. Scherer, “Tartan imu: A light foundation model for inertial positioning in robotics,” *CVPR*, pp. 22520–22529, 2025.
- [11] Y. Qiu, C. Xu, Y. Chen, S. Zhao, J. Geng, and S. Scherer, “Airio: Learning inertial odometry with enhanced imu feature observability,” *IEEE Rob. Autom. Lett.*, pp. 1–8, 2025.
- [12] Y. Wang and Y. Zhao, “Wavelet dynamic selection network for inertial sensor signal enhancement,” *Proc. AAAI Conf. Artif. Intell.*, vol. 38, no. 14, pp. 15680–15688, Mar. 2024.
- [13] R. K. Jayanth, Y. Xu, Z. Wang, E. Chatzipantazis, K. Daniilidis, and D. Gehrig, “EqNIO: Subequivariant neural inertial odometry,” in 13th Int. Conf. Learn. Represent., 2025.
- [14] J. Yuan, H. Gao, D. Dai, J. Luo, L. Zhao, Z. Zhang, Z. Xie, Y. X. Wei, L. Wang, Z. Xiao, Y. Wang, C. Ruan, M. Zhang, W. Liang, and W. Zeng, “Native sparse attention: Hardware-aligned and natively trainable sparse attention,” 2025.
- [15] X. Chen, H. Li, M. Li, and J. Pan, “Learning a sparse transformer network for effective image deraining,” in *CVPR*, June 2023, pp. 5896–5905.
- [16] X. Ding, X. Zhang, N. Ma, J. Han, G. Ding, and J. Sun, “Repyvgg: Making vgg-style convnets great again,” in *Proceedings of the IEEE/CVF Conference on Computer Vision and Pattern Recognition*, 2021, pp. 13733–13742.
- [17] H. Yan, Q. Shan, and Y. Furukawa, “Ridi: Robust imu double integration,” in *ECCV*, 2018, pp. 641–656.
- [18] S. Herath, H. Yan, and Y. Furukawa, “Ronin: Robust neural inertial navigation in the wild: Benchmark, evaluations, & new methods,” in *ICRA*, 2020, pp. 3146–3152.
- [19] D. Chen, N. Wang, R. Xu, W. Xie, H. Bao, and G. Zhang, “Rnin-vio: Robust neural inertial navigation aided visual-inertial odometry in challenging scenes,” in *ISMAR*, 2021, pp. 275–283.
- [20] W. Liu, D. Caruso, E. Ilg, J. Dong, A. I. Mourikis, K. Daniilidis, V. Kumar, and J. Engel, “Tlio: Tight learned inertial odometry,” *IEEE Rob. Autom. Lett.*, vol. 5, no. 4, pp. 5653–5660, 2020.
- [21] C. L. Gentil, F. Tschopp, I. Alzugaray, T. Vidal-Calleja, R. Siegwart, and J. Nieto, “Idol: A framework for imudvs odometry using lines,” 2020, arXiv:2008.05749.
- [22] B. Rao, E. Kazemi, Y. Ding, D. M. Shila, F. M. Tucker, and L. Wang, “Ctin: Robust contextual transformer network for inertial navigation,” *Proc. AAAI Conf. Artif. Intell.*, vol. 36, no. 5, pp. 5413–5421, Jun. 2022.
- [23] C. Chen, P. Zhao, C. X. Lu, W. Wang, A. Markham, and N. Trigoni, “Oxioid: The dataset for deep inertial odometry,” *arXiv preprint arXiv:1809.07491*, 2018.
- [24] S. M. Nguyen, L. D. Tran, D. Viet Le, and P. J. M. Havinga, “iMoT: Inertial Motion Transformer for Inertial Navigation,” *arXiv e-prints*, p. arXiv:2412.12190, Dec. 2024.